

Thermal structure of continental upper mantle inferred from *S*-wave velocity and surface heat flow

Axel H.E. Röhm, Roel Snieder*, Saskia Goes, Jeannot Trampert

Faculty of Earth Sciences, Utrecht University, Utrecht, The Netherlands

Received 20 April 2000; accepted 13 June 2000

Abstract

Results from seismic tomography provide information on the thermal structure of the continental upper mantle. This is borne out by the good agreement between tectonic age, surface heat flow and a tomographic *S*-wave velocity model for depths less than 180 km. The velocity anomalies of tomographic layers deeper than 230 km have relatively small amplitudes and show little correlation with surface heat flow or shallow velocities. We associate the drop in correlation and amplitude of the velocity perturbations between 180 and 230 km depth with the maximum thickness of the thermal boundary layer (TBL), in which larger variations in temperature and possibly composition than in the underlying convecting mantle can be sustained. Velocity profiles for different tectonic provinces are converted to temperature using mineralogical data. Both anharmonic and anelastic effects on the wave speeds are taken into account. The resulting geotherms differ most at depths of 60–120 km with variations of up to 900°C. Below 230 km, differences do not exceed 300°C. These geotherms agree well with one-dimensional conductive geotherms for the observed range of continental heat flow values using the empirical relationship that 40% of the surface heat flux stems from upper crustal radiogenic heat production. The *S*-wave velocity in the continental upper mantle appears to be adequately explained (within the uncertainties of the tomography and the conversion to temperature) by a thermal signature. A compositional component can, however, not be ruled out as it may have only a minor effect on the velocity and the heat flow. The surface heat flow is controlled by the shallow heat production and the thickness of the TBL. Seismology helps to determine the relative importance of the two factors and our results confirm the similar importance of both factors. Variations of TBL thickness could be controlled by compositional differences and/or by the effect of temperature on the rheology. © 2000 Elsevier Science B.V. All rights reserved.

Keywords: lithosphere; surface waves; tomography; heat flow; upper mantle; geothermal gradient

1. Introduction

Oceanic lithosphere is continuously recycled by mantle convection. It is formed at mid oceanic

ridges, thickens when it cools and finally subducts at plate boundaries. In contrast, continental crust does not participate in recycling. Old continental regions are many times older than the oldest existing ocean floor. They contain Archean nuclei around which younger material is accreted. Several basic questions about the continents are not yet fully answered, e.g. what is the growth rate as a function of geological time [1]? The mantle part

* Corresponding author. Present address: Department of Geophysics, Colorado School of Mines, Golden, CO 80401, USA.; E-mail: rsnieder@mines.edu

of the continental lithosphere raises some additional questions. Is it always of the same age as the continental crust and, if so, what causes this long-term stability? What is its present-day thickness? Answers to these questions depend on the adopted definition of lithosphere, which can be based on very different quantities [2–4]. Definitions which can be found in the literature refer to the mechanical lithosphere, the seismic lithosphere, the chemical lithosphere, the electrical lithosphere and the thermal lithosphere.

This study is concerned with the seismic upper mantle structure (down to the transition zone beginning at about 400 km depth) and the corresponding thermal structure. Since the low-velocity zone is often absent in stable continental regions [5,6] and since we consider smooth perturbations from a seismic reference model, we define the seismic lithosphere in this article as the region where the seismic velocity perturbations correlate with tectonic provinces and the surface heat flow. This definition includes a larger part of the mantle than, for example, the mechanical lithosphere as will become clear later when the seismic lithosphere is related to the thermal boundary layer (TBL). The TBL is viewed as the region with a predominantly conductive heat transfer.

Many different values for the thickness of the seismic continental keels are reported in the literature, ranging from several tens of kilometers beneath tectonically active regions to a few hundred kilometers below ancient cratons. There is no consensus on the maximum depth extent of continental high-velocity roots and estimates range from less than 200 km to more than 400 [2,7,8].

Variations in continental lithospheric thickness (all definitions) can be caused by several mechanisms which have distinct spatio-temporal signatures that can be used to distinguish between them.

1. Plate tectonic events, such as continental collision or rifting, thicken or thin the lithosphere accompanied by thermal disturbances and possibly also by accretion or delamination of a chemically distinct layer. The thermal relaxation time of these events is (depending on their depth) estimated to be between 15 Ma and 235 Ma [3,9]. Hence, tectonic events have a significant influence for several hundred million years, but old stable regions should be close to thermal equilibrium.
2. Mantle convection can cause undulations of the lithosphere [3].
3. Erosion has a 2-fold effect on the heat flow. First, it is accompanied by uplift which brings deeper isotherms closer to the surface. For high erosion rates of tectonically active regions with pronounced topography, this might be responsible for up to 50% of the surface heat flow [9]. Second, it removes part of the radiogenic crust, thus permanently decreasing the surface heat flux and the shallow temperature gradient. This change in the crustal blanketing effect may also influence the thickness of the TBL. This issue is addressed below in more detail.
4. A compositional root of depleted mantle material can originate through extraction of partial melt [10,11]. The reduced weight of depleted material presents an explanation for the proposed stability of the continental lithosphere.

The temporal behavior is one difference between these mechanisms. A second one is the original depth of the disturbances which is within the mechanical lithosphere for (1), below the TBL for (2), close to the surface for (3), or mainly in the lower part of the TBL for (4). Of course, these explanations do not exclude each other and a combination of the different sources is possible. From this, it should be clear that young continental regions can have a wide diversity of thermal structures, while old continental regions are expected to show less thermal variation.

Several studies have used seismic models to infer the thermal structure [12–16]. In this article, we first show the good accordance between the tomographic model of Woodhouse and Trampert [17], the compilation of surface heat flow measurements of Pollack et al. [18] and the continental regionalization of Nataf and Ricard [13], and use this to investigate the thermal structure of the continental lithosphere.

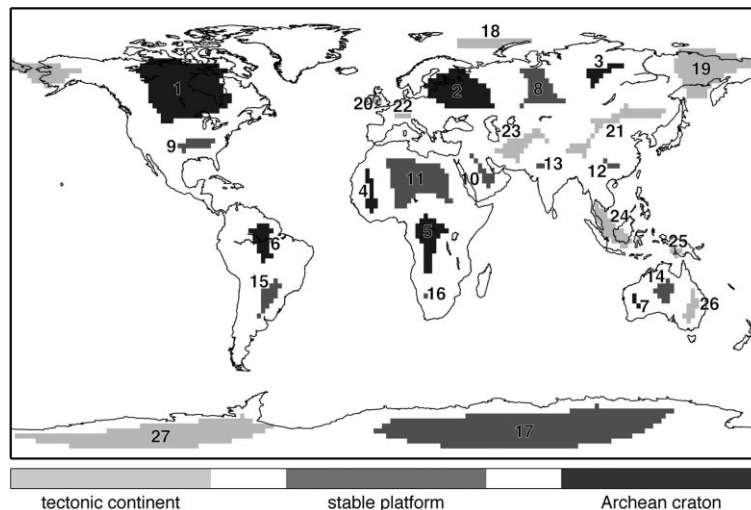


Fig. 1. Continental tectonic provinces after the 3SMAC regionalization [13] marked by the gray shades. Shown is only the inner part of each province that is at least 5° away from any other province.

2. Seismic tomography and tectonic regionalization

Surface wave dispersion measurements and seismic tomography have revealed the correlation between tectonic setting and lithospheric seismic velocities, with old cratons showing the highest, and tectonically active regions having relatively low velocities [5,19,20]. In this study, the tomographic model of Woodhouse and Trampert [17] is used to analyze the continental upper mantle structure above 400 km depth.

Their model presents an improved depth resolution over previous models. This is achieved by incorporating fundamental mode Love and Rayleigh wave dispersion measurements in the period range 40–150 s together with a large waveform data set similar to that employed in the construction of earlier mantle models [20]. The surface wave data set corresponds to that of Trampert and Woodhouse [17] and consists of 62 141 Love and Rayleigh wave measurements. They showed that this data set could resolve unbiased structure at least up to degree 16. Compressional velocity ($\delta v_p/v_p$) is scaled to shear velocity ($\delta v_s/v_s$) which is parameterized in spherical harmonics up to degree 16 and cubic splines as a function of depth. The knots are placed at increasing depth intervals (24, 74, 128, 188, 253, 323, 400, 484... km) resulting in a vertical resolution length of about 50–70 km in

the first 400 km of the model, the area of our primary interest. This improved vertical resolution in the upper part of the mantle is primarily achieved by the incorporation of short period surface waves. Surface topography and bathymetry have been specified while crustal thickness has been inverted for. Within the uncertainties of the tomographic model, the inverted crust and the crustal model of Mooney et al. [21] give the same results.

To investigate the correlation between tectonic region and deeper mantle structure, the tomographic model is compared with the regionalization of model 3SMAC [13], which divides continental areas into three different tectonic types: Archean cratons, stable platforms and tectonic continents (Fig. 1). The resolution of the tomographic model does not justify a division into more types which would yield smaller provinces. The $2^\circ \times 2^\circ$ lateral discretization of the model is fine enough for the comparison with the tomographic model.

We calculated an average velocity profile for each region from the tomographic model of Woodhouse and Trampert [17]. Since the tomographic model has a finite lateral resolution, only the area of each province, which is located at a distance of at least 5° from the boundary to another province, is used. These areas are shown in

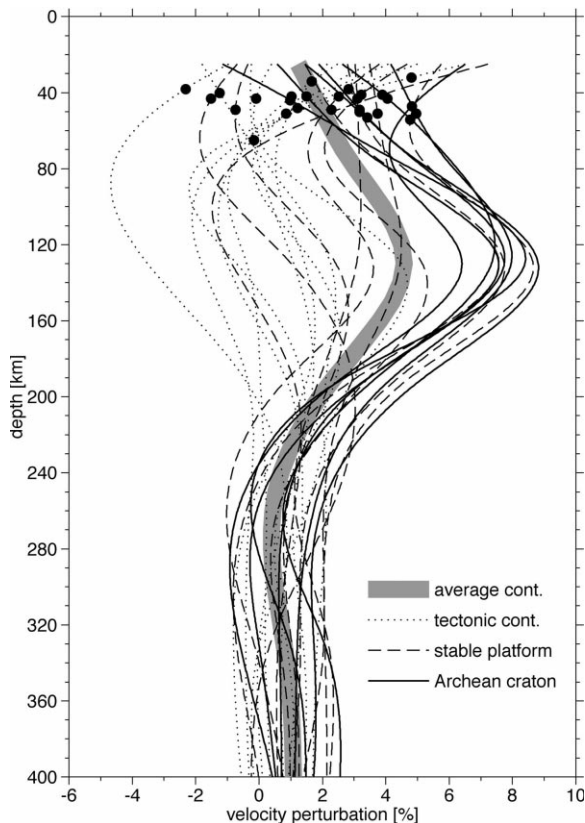


Fig. 2. Velocity profiles are obtained by averaging the velocity perturbations of the global tomographic model of Woodhouse and Trampert [17] over the interior regions of the provinces from the 3SMAC continental regionalization shown in Fig. 1. The dots denote the maximum crustal thicknesses for each province which are used for the crustal correction of the tomography. The global average velocity perturbation (degree 0 term of the spherical harmonic expansion) for each depth is subtracted. Different line textures denote the three types of continental provinces. The very thick gray line displays the mean profile of all continental regions with a distance of at least 5° from oceanic lithosphere.

Fig. 1 in gray shades. Fig. 2 shows the corresponding velocity profiles. The strongest feature is the decrease in variation of the seismic velocity from more than 10% at shallow depths to less than 4% below a depth of 230 km. All seven Archean profiles (no. 1–7 in Fig. 1) from five different continents show a striking similarity. In the upper 200 km, they are clearly separated from the tectonic regions which show a much larger diver-

sity. The profiles for stable platforms span almost the complete range from the fast profiles of Archean cratons to the slow profiles of tectonic continents. Closer inspection of the stable platform provinces reveals possible causes for this broad range. The three fastest profiles, which show the same velocities as the Archean provinces, are no. 9 (Eastern USA), which also shows a lower median surface heat flow of 47 mW/m^2 compared to other provinces of the same type (Table 1), no. 14 (Central Australia), which forms in the tomographic model one fast anomaly together with the Archean region no. 7, and no. 17 (Eastern Antarctica), which is a Precambrian shield. On the other side are the three slowest profiles of stable platforms: no. 10 (Arabian peninsula), which is surrounded at all sides by active plate boundaries, no. 11 (Northern Africa), which contains the Hoggar and Tibesti hotspots [22,23], and no. 12 (China), which is in active extension [24]. We find from the tomographic model (Fig. 2) that the thickness of the seismic lithosphere, defined as the upper mantle region which shows strong variations of seismic velocity related to surface tectonics, is slightly more than 200 km.

The average profile of all continental regions with a distance of at least 5° from oceanic lithosphere, shown as the thick gray line in Fig. 2, is positive at all depths down to 400 km. Since the global average is subtracted, this implies that the *S*-wave velocity below oceans is on average slower than the subcontinental velocity. Relative to the global average, i.e. zero in Fig. 2 for all depths, some provinces have fast velocity perturbations of up to about 2% throughout the upper mantle. This can partly explain why other studies [7,8] found much deeper roots than the 200 km found in this study. However, this type of anomaly is not correlated with age (Fig. 2).

The differences between profiles above and below a depth of about 200 km are even more striking in the correlation of the velocity perturbations at two different depths. Fig. 3 shows the correlation of the velocity field of continental area (with a distance of at least 5° from the oceans) between a depth of 100 km and a second depth indicated by the vertical axis. The correlation profile can be divided into two regions. Between 60 and 180 km

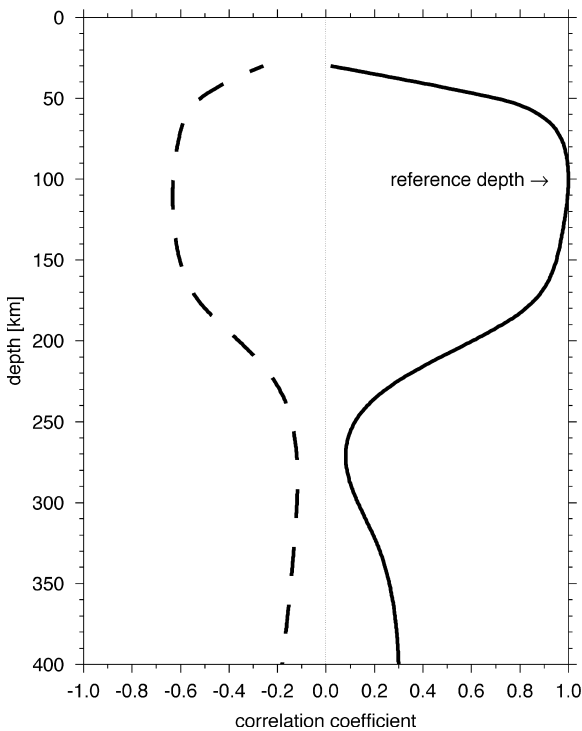


Fig. 3. Correlation coefficient between S -wave velocity at the depth given on the ordinate and the S -wave velocity at 100 km depth (solid line) and averaged surface heat flow (dashed line). Only continental areas with a distance of at least 5° from oceanic crust are included in the calculation. The averaging of heat flow values is explained in the text.

depth, the correlation coefficient is higher than 0.8. Below 230 km depth, the correlation drops to values between 0.1 and 0.3. The transition from high to low correlations marks the depth of the seismic lithosphere, which we have defined as the region where the velocity correlates with surface tectonics. The low values of the correlation coefficient at depths less than 60 km is caused

by crustal effects since the crustal correction is not applied in the calculation for Fig. 3. The very small correlation between the seismic lithosphere and the underlying structure suggests that the strong shallow anomalies are not controlled from below by the convection but have a shallow origin, i.e. within the upper 200 km. However, the influence of plume activity cannot completely be ruled out because mantle plumes could be too small in size or temperature contrast to be resolved in the tomographic model.

3. Surface heat flow

Surface heat flow measurements form another, completely independent, data source giving valuable constraints on the thermal structure of the crust and shallow mantle. Several studies [18,25–27] have found a systematic decrease of surface heat flow with the age of tectonic provinces. For this study, the global heat flow compilation of Pollack et al. [18] is used.

Three points concerning the heat flow data have to be considered in the comparison: (1) there is a considerable amount of scatter in the measurements due to environmental problems, e.g. water circulation and past climatic changes, and difficulties with early conductivity determinations [26], (2) the surface heat flow can have large changes over short distances due to the local geology and topography, and (3) the measurements are highly unevenly distributed over the Earth's surface. A simple pointwise comparison for all measurement sites of surface heat flow and volume-averaged quantities, such as seismic velocities revealed by waveform tomography, is complicated by each of the three points listed above. Appro-

Table 1

Median values for surface heat flow of different provinces, 99% confidence intervals around the median and the mean absolute deviations about the median

	Median (mW/m ²)	99% confidence interval (mW/m ²)	Mean absolute deviation (mW/m ²)
Continental area	55	54–56	26.1
Archean craton	42	40–44	10.8
Stable platform	54	51–56	11.3
Tectonic continents	76	70–81	24.3

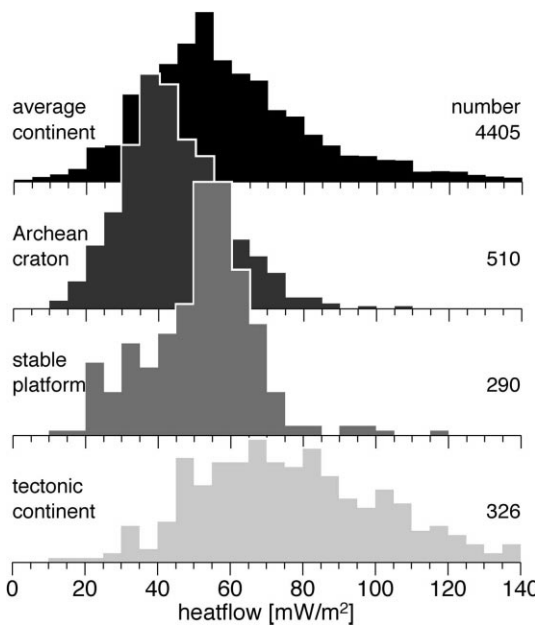


Fig. 4. Histograms for continental heat flow measurements and HF measurements for the interiors of the three different types of tectonic provinces. Histograms are normalized; the number of measurements is given on the right side of each histogram.

priate averaging methods have to be used to construct average heat flow values for larger areas that can be used for the comparison. In order to suppress any overweighting from clustered measurement points, we first averaged all heat flow measurements within $20 \text{ km} \times 20 \text{ km}$ cells.

Fig. 4 shows histograms of heat flow values for the three different types of continental provinces and for all continental values. Just as for the velocity profiles of Fig. 1, only measurements with a distance of at least 5° from the tectonic boundaries are used. Median values and absolute deviation about the median are listed in Table 1.

For comparison with the tomographic model, the heat flow values were averaged a second time with the aim to estimate the average heat flow of an area similar in size to the resolution of the velocity model. For this, a heat flow value was assigned to each node of a $2^\circ \times 2^\circ$ coordinate grid if at least one $20 \text{ km} \times 20 \text{ km}$ average value was within 110 km and three values were within 550 km distance of the node. All nodes on con-

tinents that were more than 5° away from the oceans and that received an averaged heat flow estimate were used in the subsequent calculation of the correlation coefficient between surface heat flow and *S*-wave velocity perturbation as a function of depth. The result is shown in Fig. 3 as the dashed line.

This correlation function has almost the same shape as the correlation function of two different depth layers of the tomographic model but has the opposite sign and a lower amplitude. The negative sign is due to the anticorrelation between temperature and seismic velocities. Considering the scatter in the heat flow measurements and a non-linear relation between temperature and *S*-wave velocity, the anticorrelation is remarkably large. The strong anticorrelation between heat flow and velocity between 60 km and 180 km depth suggests that the velocity perturbations are predominantly caused by temperature effects. The small correlation coefficients above 60 km depth are again caused by crustal effects. Yan et al. [15] have used *S*-wave velocities at 150 km depth to predict global heat flow and found a qualitative agreement to the observed global heat flow pattern for the lowest 6° of a spherical harmonic expansion. The strong anticorrelation in Fig. 3 shows that this is also valid for continental regions only and at smaller scales.

4. Constraints on temperatures from *S*-wave velocity

The strong anticorrelation between heat flow and seismic velocity favors a thermal interpretation of the tomographic model. Other studies [16,28,29] also confirm that the expected effect of reasonable variations in upper mantle composition as found in xenoliths is of minor importance compared to the expected temperature effect and is probably of similar magnitude as the uncertainties in the tomography. In our subsequent analysis, we concentrate on the mantle below 60 km depth to avoid complications due to the presence of crustal material and give an interpretation in terms of temperatures alone.

Following the procedure developed by Goes et

al. [16], the conversion of *S*-wave velocity to temperature is carried out by using laboratory measurements of density and the elastic moduli for various mantle minerals. These values are extrapolated to mantle temperature and pressures under the infinitesimal strain approximation. (Finite strain theory would be more correct, but a comparison has shown that the error introduced is relatively small for our depth range of interest (Vacher, personal communication)). The elastic moduli for an average mantle composition are determined by using the Voigt–Reuss–Hill averaging method. Anelasticity, which is an important effect for finite frequencies [30] but unfortunately less well constrained by experimental data, is also taken into account. The importance of anelasticity increases with temperature and does not allow the application of a linear relation between velocity and temperature anomalies. For further details, including the mineralogical data used, we refer to Goes et al. [16].

Due to the non-linear relation between velocity and temperature, the conversion has to be done using absolute velocities rather than velocity perturbations. This causes an extra difficulty, since the reference model used for the tomography [31] incorporates an anisotropic layer down to the Lehmann discontinuity at 220 km depth. The equivalent isotropic PREM model also contains this discontinuity in form of a 5% step of *S*-wave velocity. Many different explanations have been proposed for the Lehmann discontinuity, such as a chemical boundary or the base of a partially molten layer [32], or an anisotropic layer above the discontinuity [5,32,33]. The global occurrence of the discontinuity is questioned and little seismological evidence exists that the corresponding isotropic velocities are discontinuous at this depth, e.g. the global waveform stacks of Shearer [34] show the 410, 520 and 660 km discontinuities but not the Lehmann discontinuity.

It would be best to include this discontinuity in our modeling, e.g. through a discontinuous composition or rheology. However, the lack of a clear thermodynamic understanding of it makes this approach impossible. We have decided, as a second-best approach, to slightly modify the seismic reference model. If the changes of the reference

model are small, the phase velocities and the sensitivity kernels of the surface waves remain similar and a tomographic inversion yields only slightly different velocity perturbations. We verified that these changes are much smaller than the velocity perturbations displayed in Fig. 2. Using PREM as reference model, the absolute *S*-wave velocity V for a profile i is given by:

$$V_i = V_{\text{PREM}} + \delta V_{\text{global}} + \delta V_i$$

where V_{PREM} is the PREM *S*-wave velocity, δV_{global} is the global mean velocity perturbation from PREM found in the inversion (i.e. the degree 0 term of the spherical harmonic expansion) and δV_i is the velocity perturbation as displayed in Fig. 2. Using the absolute velocities V_i would yield discontinuous temperatures due to the discontinuity in V_{PREM} . Therefore, we have chosen to introduce a new, thermally based, reference model. Since all Archean profiles are very similar (Fig. 2) and also Archean heat flow values show the least scatter (Table 1), an obvious choice is to specify a geotherm representative for Archean cratons. This geotherm is calculated using the method of Chapman [35] for the median Archean heat flow of 42 mW/m². Below the intersection of the conductive geotherm with the adiabat (potential temperature of 1200°C) at about 200 km depth, temperatures along the adiabat are taken for the geotherm. This gives new absolute velocity profiles V_i' :

$$V_i' = V(T_{\text{Archean}}) - \delta V_{\text{Archean}} + \delta V_i$$

$V(T_{\text{Archean}})$ is the velocity profile calculated from the Archean reference geotherm and $\delta V_{\text{Archean}}$ the mean Archean velocity perturbation (weighted by the area of each province). The relatively cold adiabat was chosen for two reasons. First, as can be seen from Fig. 2, continental regions at depths below 200 km are approximately 1% faster than the global average and Archean cratons are on average slightly faster than average continental regions (small positive correlation coefficient in Fig. 3). Therefore, if no lateral variation in composition is assumed, temperatures below Archean provinces are somewhat lower than the global

average. The second reason is that for a colder adiabat, the new reference model ($V(T_{\text{Archean}}) - \delta V_{\text{Archean}} - \delta V_{\text{global}}$) is closer to the reference model of the tomography (V_{PREM}). For each profile δV_i in Fig. 2 the absolute velocity profile V_i' was calculated and converted to temperature. The result is shown in Fig. 5.

To demonstrate the influence of different compositions and the anelastic effect, we selected three velocity profiles for provinces 1, 8 and 19 (see Fig. 1), one of each tectonic type. The corresponding temperatures were calculated with respect to two different compositions and two Q models. One composition represents an average continental lherzolite based on xenolith data which is depleted relative to a primitive mantle, the other a primitive garnet lherzolite [28]. The compositions are described in Table 2. The Q models represent an average model (Q_1 of Goes et al. [16]; after model 2 of Sobolev et al. [12]) calibrated to seismic data and a fully experimental Q model which is a relatively strong estimate of temperature dependence (Q_2 of Goes et al. [16]; after Berckhemer et al. [36]). Fig. 6 shows the resulting geotherms. The solid lines show the three profiles for the preferred composition (average continental garnet lherzolite, Q_1), also used for Fig. 5. A change of composition to a primitive mantle (dotted line, same Q model) shows only negligible effects. A change to the anelastic model Q_2 (long dashed line) has also only small effects, except for the very high temperatures of the tectonic profile around 100 km depth. The very slow velocities of tectonic provinces in this depth region give temperatures which are about 100°C lower for the stronger anelastic effect of model Q_2 than the temperatures computed for model Q_1 . It should be noted that the Archean profiles show almost no difference because the profiles are so close to the fixed new

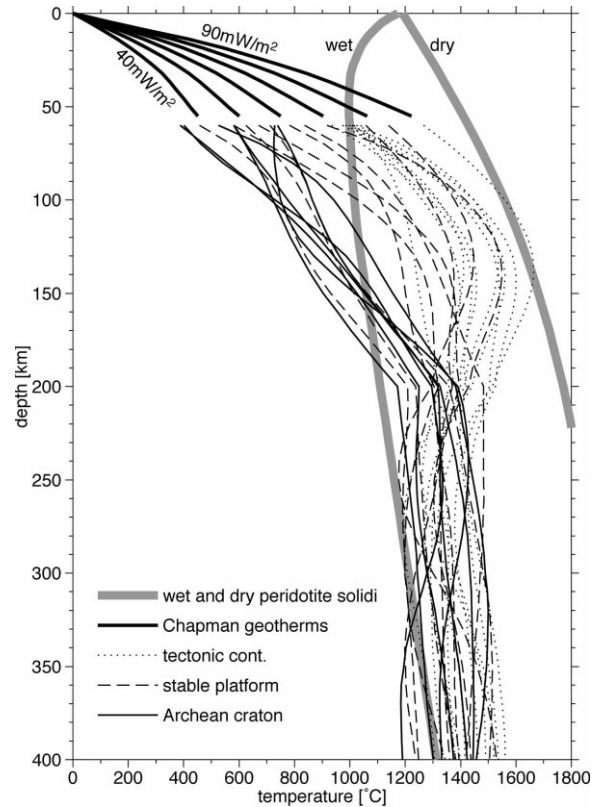


Fig. 5. Temperature profiles calculated for the velocity profiles from Fig. 2. In the upper, 55 km geotherms after Chapman [35] for surface heat flows of 40–90 mW/m² are shown. The thick gray lines show a wet and dry peridotite solidus taken from Thompson [50].

reference model. The short dashed line illustrates a shift of the reference model; the temperatures of the reference Archean geotherm, which has been converted to the reference velocity profile, were increased by 100°C everywhere. This results in a shift of the Archean profile by the same amount. The other profiles, especially of tectonic provinces at shallow depths, show a somewhat lower in-

Table 2
Volume fraction of minerals in the two mantle rocks tested in Fig. 6

Garnet lherzolite	Olivine Mg ₂ SiO ₄	Orthopyroxene MgSiO ₃	Clinopyroxene CaMgSi ₂ O ₆	Garnet Mg ₃ Al ₂ Si ₃ O ₁₂
average	0.65 volume fraction of Fe for all minerals: 0.09	0.28	0.03	0.04
primitive	0.58 volume fraction of Fe for all minerals: 0.11	0.18	0.10	0.14

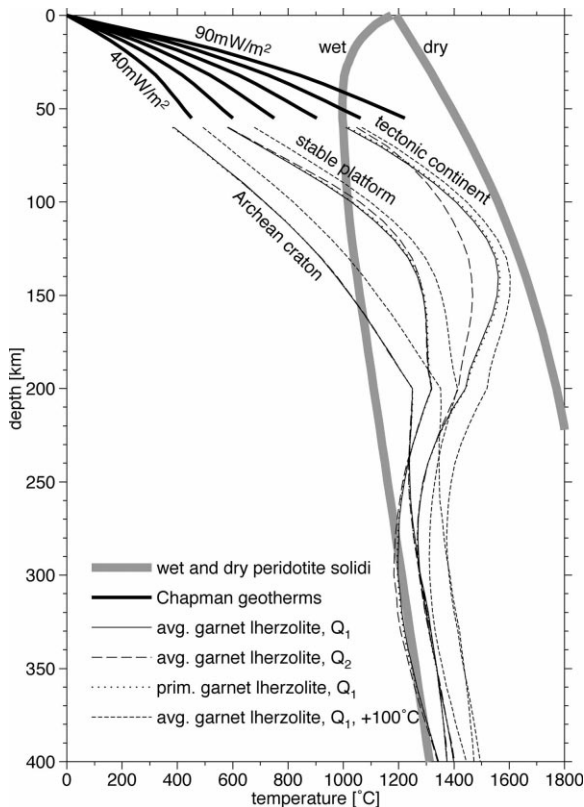


Fig. 6. The three profiles for regions no. 1, 8 and 19 of Fig. 1 converted to temperatures for different compositions, anelastic effects and a change of reference geotherm. Geotherms in upper 55 km and solidi are the same as in Fig. 5.

crease due to the anelastic effect. This shows that an erroneous estimate of the average continental composition has only little effect on the relative position of the computed geotherms, whereas a wrong thermal reference model can shift all geotherms systematically to higher or lower temperatures. Of course, we have not yet discussed the effect of a laterally varying composition. This could shift some of the geotherms by amounts comparable to the variation of the reference model (by 100°C), which is much less than the total observed variation.

5. Comparison with heat flow-derived geotherms

The geotherms in Fig. 5 for most tectonic continents and some stable platforms show a maxi-

mum at depths of about 130 km. This might be surprising because for an upward heat, flow temperatures increase monotonically with depth. This could be due to plume activity in these relatively hot regions. Geotherms calculated from convection models often overshoot the adiabat due to the spreading plume heads at the base of the boundary layer [37]. However, it could also be caused by the presence of partial melt. If the mantle in these regions was partially molten, the calculated temperatures are overestimated. Since the maxima are close to the dry solidus, this is a likely explanation as well. About 4% of melt would be needed to obtain geotherms which are about 200°C colder around the maxima. A different anelasticity model would have a similar influence. Fig. 6 demonstrates that invoking a stronger anelastic effect, such as in model Q_2 , also decreases the estimated temperatures in this temperature–depth region.

Kinks can be seen in the temperature profiles of Figs. 5 and 6 at 200 km depth which are artifacts that originate from the abrupt transition from a conductive geotherm to an adiabat in the reference profile. In reality, the geotherms are expected to be smooth across this transition. We concentrate on the gross pattern in Fig. 5 and point out two robust features. First, there is a large range of temperatures at a depth of 60 km of about 900°. Second, tectonic regions reach the adiabat at depths shallower than 80 km as opposed to Archean regions which reach the adiabat at depths of around 200 km.

First, the temperature variation at 60 km depth matches the range given by the Chapman [35] geotherms for surface heat flow.

Fig. 7 shows the geotherms for surface heat flow values every 10 mW/m² between 40 and 90 mW/m² for three different one-dimensional thermal models which differ only in the distribution of radiogenic elements. The frame in the center shows geotherms as proposed by Chapman [35] and one of these was used as a reference for the calculations of the profiles shown in Fig. 5. These geotherms for steady-state conductive heat transfer use the surface heat flow as the only parameter to which the heat production is linked by the relationship that 40% is attributed to upper crus-

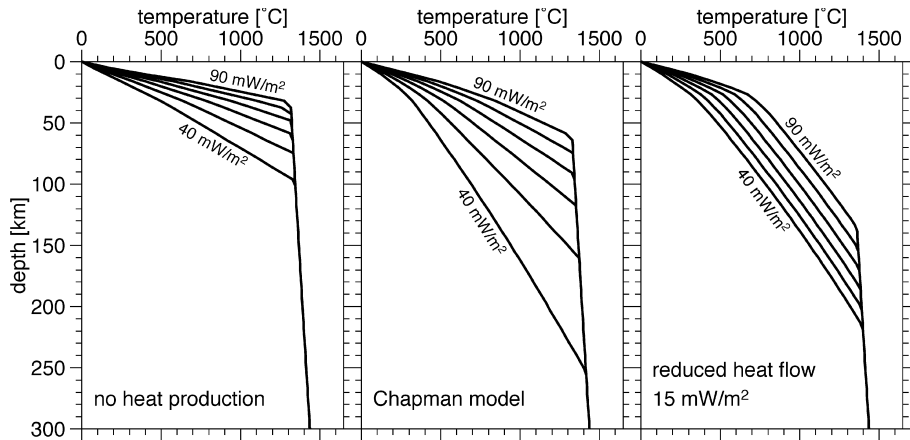


Fig. 7. Three different geotherm families for surface heat flows of 90, 80, 70, 60, 50 and 40 mW/m^2 (top down). All geotherms are truncated by the 1300°C adiabat. The left panel displays geotherms for a crust without any heat production. The middle panel shows geotherms proposed by Chapman [35]. Geotherms in the right panel have all the same reduced mantle heat flow of 15 mW/m^2 .

tal radiogenic heat sources and 60% to deeper sources (the total crustal contribution is 57% and 44% for a surface heat flow of 40 mW/m^2 and 90 mW/m^2 , respectively) [38,39]. The Chapman geotherms [35] diverge in the crust and shallow mantle and predict temperature differences of more than 500°C below the crust. This large variation is also found in geothermobarometric data obtained of xenoliths from different regions [40–42]. At high temperatures in greater depths, heat transfer is dominated by advection which is incorporated by truncating the conductive geotherms with an adiabat with a potential temperature of 1300°C although potential temperatures of 1400°C and 1280°C have been reported as well [43,44]. These uncertainties in the thermal properties could cause a systematic shift of all geotherms of Fig. 5 by at most 100–200°C.

Next to the middle panel of Fig. 7, two extreme end-members of possible geotherm families are shown. They are calculated for the same parameters with the only difference in the amount of crustal heat production. The left plot shows geotherms for the case without any crustal heat production. These geotherms are almost straight lines (some deviation from straight lines is caused by changes in the thermal conductivity) until they cross the adiabat and their slope is proportional to the surface heat flow. In other words, if the

temperature of the convecting mantle follows an adiabat, the surface heat flow is solely determined by the thickness of the conductive boundary layer. If it is assumed that the seismic anomalies shown in Fig. 2 are mainly caused by temperature effects (since compositional variations are very unlikely to explain such large variations), these geotherms can be ruled out as an explanation because they do not explain the differences in seismic velocity below 100 km depth.

Another extreme family is the case in which the mantle heat flow for all geotherms is the same. Estimates for the non-radiogenic component of the surface heat flow range from 6 mW/m^2 [45] to 25 mW/m^2 [26]. In this example, a value of 15 mW/m^2 was used. The different surface heat flow is in this example only caused by differences in the crustal heat production. Comparison of these geotherms with the ones from Fig. 5 shows that the differences in temperature are far too small. Additionally, these geotherms would not allow partial melting for depths less than 100 km which is expected for many tectonically active regions.

Therefore, continental geotherms are determined by a combination of (1) the crustal heat production and (2) the thickness of the conductive boundary layer. A variable thickness of the TBL can be seen in Fig. 5 but this thickness alone is

not sufficient to explain the large variation of observed heat flow values. The Chapman geotherm family, which includes a correlated variation in both, gives temperatures very similar from what is found in Fig. 5 and is thus consistent with the tomographic *S*-velocity. The temperature variations are largest at shallow depths around 60 km where they reach a maximum of about 900°C. Below the seismic lithosphere, temperature variations do not exceed 300°C.

6. Discussion

Different heat fluxes lead to diverging geotherms but at depths where heat transfer is dominated by material transport and not by conduction, the temperatures come closer to a mean mantle adiabat. The Chapman geotherm family [35] for surface heat flow values between 42 and 90 mW/m² covers a broad temperature–depth space (down to 225 km depth and up to 900°C temperature variation). This depth range is in good accordance with the seismic lithosphere, which was defined as the region of strong velocity variation related to tectonic provinces, obtained from Figs. 2 and 3. Additionally, the temperature range explains the *S*-velocity difference of up to 12% found in the lithosphere.

Variations of the surface heat flow are sometimes mainly ascribed to the thickness of the continental roots or to differences in the crustal heat production [46–48]. Seismic studies yield important extra information to resolve this. The good correspondence of our results with the Chapman geotherms suggests that both causes are of similar importance and correlated. The extreme geotherm families depicted in the left and right panels of Fig. 7, which involve only one cause, cannot explain the seismic velocity variations. Therefore, both mechanisms must be operative. The crust is enriched in radiogenic elements, mainly Cs, Rb, Th and U, relative to the depleted mantle because most of these elements are incompatible, which means that they do not fit readily into crystal lattices, and thus are easily removed from the mantle by the extraction of partial melt, in which they are concentrated. Erosion, in turn, removes

the enriched crustal rocks exposed to the surface from a particular region. Thus, differentiation of mantle material and erosion are the factors determining the crustal heat production.

The thickness of the TBL influences the temperature gradient and thus the conductive heat flow. One question that remains is what causes this variation in thickness. Since the seismic velocities in the lithosphere have only a small correlation with the velocities below the TBL (Fig. 3), a deep cause, e.g. mantle convection, is unlikely. Two other possibilities exist. First, the TBL could be determined by a compositionally different layer. To explain the stability and geoid signature of continental lithosphere, differentiation processes are needed that generate a mantle residue, which has a lower density, a higher solidus temperature and a higher viscosity [10,11,49], and thus forms a layer that does not participate in convection. This chemical layer could impose the TBL. Second, the thickness could be determined thermally by the amount of crustal thermal blanketing. Little shallow heat production results in a smaller temperature increase through the crust and thus more efficient cooling of the lower lithosphere resulting in a thick TBL caused by a temperature-dependent rheology. The opposite would be true for high concentrations of heat producing elements in the crust. If this explanation is correct, then the concentration of radiogenic elements would be the dominant controlling factor for the TBL in thermal equilibrium by influencing the temperature directly through heat production and indirectly by determining the thickness of the TBL.

Our results do not support the hypothesis that the convection pattern dictates the thermal structure of the TBL. On the contrary, they point to a top-down cause–effect relation in which variations in the shallow radiogenic heat production produce the large-scale velocity anomalies in the shallow mantle. Beneath old cratons, where erosion has removed most of the upper crustal radiogenic elements, a thick TBL, associated with fast velocity anomalies, has formed. In addition, variations in the thickness of the TBL play a role as well. These variations could be caused by the effect of temperature on the TBL through a temperature-depen-

dent rheology, but other causes such as compositional variations cannot be ruled out on the basis of the data used in this study.

Acknowledgements

We thank Hana Cizkova, Frederic Deschamps, Dirk Kraaijpoel, Everhard Muyzert, Jeroen de Smet, Christophe Sotin and Volker Steinbach for many beneficial discussions and J.-P. Montagner and H.-C. Nataf for helpful reviews. This research was supported by the Netherlands Organization for Scientific Research (NWO) through the Pioneer project PGS 76-144. [AC]

References

- [1] B.F. Windley, *The Evolving Continents*, John Wiley and Sons, 1995.
- [2] D.L. Anderson, *Geophysics of the Continental Mantle: an Historical Perspective*, Continental Mantle, M.A. Menzies, Clarendon Press, Oxford, 1990, pp. 1–30.
- [3] H. Schmeling, G. Marquart, The influence of second-scale convection on the thickness of continental lithosphere and crust, *Tectonophysics* 189 (1991) 281–306.
- [4] D.L. Anderson, Lithosphere, asthenosphere, and perisphere, *Rev. Geophys.* 33 (1995) 125–149.
- [5] H.-C. Nataf, I. Nakanishi, D.L. Anderson, Measurements of mantle wave velocities and inversion for lateral heterogeneities and anisotropy, 3. Inversion, *J. Geophys. Res.* 91 (1986) 7261–7307.
- [6] A.L. Lerner-Lam, T.H. Jordan, How thick are continents?, *J. Geophys. Res.* 92 (1987) 14007–14026.
- [7] T.H. Jordan, The continental tectosphere, *Rev. Geophys. Space Phys.* 13 (1975) 1–12.
- [8] J. Polet, D.L. Anderson, Depth extent of cratons as inferred from tomographic studies, *Geology* 23 (1995) 205–208.
- [9] I. Vitorello, H.P. Pollack, On the variation of continental heat flow with age and thermal evolution of continents, *J. Geophys. Res.* 85 (1980) 983–995.
- [10] T.H. Jordan, Structure and formation of the continental tectosphere, *J. Petrol.* (1988) Special Lithosphere Issue, 11–37.
- [11] J.H. deSmet, A.P. vandenBerg, N.J. Vlaar, Stability and growth of continental shields in mantle convection models including recurrent melt production, *Tectonophysics* 296 (1998) 15–29.
- [12] S.V. Sobolev, H. Zeyen, G. Stoll, F. Werling, R. Altherr, K. Fuchs, Upper mantle temperatures from teleseismic tomography of French Massif Central including effects of composition, mineral reactions, anharmonicity, anelasticity and partial melt, *Earth Planet. Sci. Lett.* 139 (1996) 147–163.
- [13] H.-C. Nataf, Y. Ricard, 3SMAC: an a priori tomographic model of upper mantle based on geophysical modeling, *Phys. Earth Planet. Int.* 95 (1996) 101–122.
- [14] Y. Ricard, H.-C. Nataf, J.P. Montagner, The three-dimensional seismological model a priori constrained: Confrontation with seismic data, *J. Geophys. Res.* 101 (1996) 8457–8472.
- [15] B. Yan, E.K. Graham, K.P. Furlong, Lateral variations in the upper mantle thermal structure inferred from three-dimensional seismic inversion models, *Geophys. Res. Lett.* 16 (1989) 449–452.
- [16] S. Goes, R. Govers and P. Vacher, Shallow mantle temperatures under Europe from *P* and *S* wave tomography, *J. Geophys. Res.* (1999) (in press).
- [17] J.H. Woodhouse and T. Trampert, Global upper mantle structure inferred from surface wave and body wave data, *EOS Trans. AGU* (1995) F422.
- [18] H.N. Pollack, S.J. Hurter, J.R. Johnson, Heat flow from the earth's interior: analysis of the global data set, *Rev. Geophys.* 31 (1993) 267–280.
- [19] I. Nakanishi, D.L. Anderson, World-wide distribution of group velocity of mantle Rayleigh waves as determined by spherical harmonic inversion, *Bull. Seismol. Soc. Am.* 72 (1982) 1185–1194.
- [20] J.H. Woodhouse, A.M. Dziewonski, Mapping the upper mantle: three-dimensional modeling of earth structure by inversion of seismic waveforms, *J. Geophys. Res.* 89 (1984) 5953–5986.
- [21] W.D. Mooney, G. Laske, T.G. Masters, Crust5.1; a global crustal model at 5 degrees×5 degrees, *J. Geophys. Res.* 103 (1998) 727–747.
- [22] M.A. Richards, B.H. Hager, N.H. Sleep, Dynamically supported geoid highs over hotspots: Observation and theory, *J. Geophys. Res.* 93 (1988) 7690–7708.
- [23] A. Yamaji, Periodic hotspot distribution and small-scale convection in the upper mantle, *Earth Planet. Sci. Lett.* 109 (1992) 107–116.
- [24] S.A. Gilder, G.R. Keller, M. Luo, P.C. Goodell, Timing and spatial distribution of rifting in China, *Tectonophysics* 197 (1991) 225–243.
- [25] D.S. Chapman, H.N. Pollack, Global heat flow: a new look, *Earth Planet. Sci. Lett.* 28 (1975) 23–32.
- [26] J.G. Sclater, C. Jaupart, D. Galson, The heat flow through oceanic and continental crust and the heat loss of the Earth, *Rev. Geophys.* 18 (1980) 269–311.
- [27] J.G. Sclater, B. Parsons, C. Jaupart, Oceans and continents: similarities and differences in the mechanisms of heat loss, *J. Geophys. Res.* 86 (1981) 11535–11552.
- [28] T.H. Jordan, Mineralogies, densities and seismic velocities of garnet lherzolites and their geophysical implications, in: F.R. Boyd and H.O.A. Meyer (Eds.), *The Mantle Sample: Inclusions in Kimberlites and Other Volcanics*, AGU, Washington, DC, 1979, pp. 1–14.
- [29] I. Jackson and S.M. Rigden, Composition and temper-

- ature of the Earth's mantle: seismological models interpreted through experimental studies of Earth minerals, in: I. Jackson (Ed.), *The Earth's Mantle: Composition, Structure and Evolution*, Cambridge Univ. Press, 1998, pp. 405–460.
- [30] S. Karato, Importance of anelasticity in the interpretation of seismic tomography, *Geophys. Res. Lett.* 20 (1993) 1623–1626.
- [31] A.M. Dziewonski, D.L. Anderson, Preliminary reference Earth model, *Phys. Earth Planet. Int.* 25 (1981) 297–356.
- [32] S. Karato, On the Lehmann discontinuity, *Geophys. Res. Lett.* 19 (1992) 2255–2258.
- [33] J.-P. Montagner, T. Tanimoto, Global upper mantle tomography of seismic velocities and anisotropies, *J. Geophys. Res.* 96 (1991) 20337–20351.
- [34] P.M. Shearer, Seismic imaging of upper-mantle structure with new evidence for a 520-km discontinuity, *Nature* 344 (1990) 121–126.
- [35] D.S. Chapman, Thermal gradients in the continental crust, in: J.B. Dawson, D.A. Carswell, J. Hall and K.H. Wedepohl (Eds.), *The Nature of the Lower Continental Crust*, Geological Society Special Publication 24, 1986, pp. 63–70.
- [36] H. Berckhemer, W. Kampfman, E. Aulbach, H. Schmeling, Shear modulus and Q of forsterite and dunite near partial melting from forced oscillation experiments, *Phys. Earth Planet. Int.* 29 (1982) 30–41.
- [37] G.T. Jarvis and W.R. Peltier, Convection models and geophysical observations, in: W.R. Peltier (Ed.), *Mantle Convection; Plate Tectonics and Global Dynamics 7*, Gordon and Breach Science Publishers, Montreux, 1989, pp. 479–593.
- [38] R.F. Roy, D.D. Blackwell, F. Birch, Heat generation of plutonic rocks and continental heat flow provinces, *Earth Planet. Sci. Lett.* 5 (1968) 1–12.
- [39] H.N. Pollack, D.S. Chapman, On the regional variation of heat flow, geotherms, and lithospheric thickness, *Tectonophysics* 38 (1977) 279–296.
- [40] S.Y. O'Reilly, W.L. Griffin, A xenolith-derived geotherm for southeastern Australia and its geophysical implications, *Tectonophysics* 111 (1985) 41–63.
- [41] P. Bertrand, C. Sotin, J.-C.C. Mercier, E. Takahashi, From the simplest chemical system to the natural one: garnet peridotite barometry, *Contrib. Mineral. Petrol.* 93 (1986) 168–178.
- [42] R.L. Rudnick, W.F. MacDonough, R.J. O'Connell, Thermal structure, thickness and composition of continental lithosphere, *Chem. Geol.* 145 (1998) 395–411.
- [43] D.L. Anderson, J.D. Bass, Mineralogy and composition of the upper mantle, *Geophys. Res. Lett.* 11 (1984) 637–640.
- [44] D. McKenzie, M.J. Bickle, The volume and composition of melt generated by extension of the lithosphere, *J. Petrol.* 29 (1988) 625–679.
- [45] R.L. Rudnick, D.M. Fountain, Nature and composition of the continental crust: A lower crustal perspective, *Rev. Geophys.* 33 (1995) 267–309.
- [46] A.A. Nyblade, H.N. Pollack, A comparative study of parameterized and full thermal-convection models in the interpretation of heat flow from cratons and mobile belts, *Geophys. J. Int.* 113 (1993) 747–751.
- [47] P. Morgan, Crustal radiogenic heat production and the selective survival of ancient continental crust, *Proceedings of the fifteenth lunar and planetary science conference*, *JGR*, 90, 1995, pp. C561–C570.
- [48] A. Lenardic, On the heat flow variation from Archean cratons to Proterozoic mobile belts, *J. Geophys. Res.* 102 (1997) 709–721.
- [49] M.-P. Dion, L. Fleitout, U. Christensen, Mantle convection and stability of depleted and undepleted continental mantle, *J. Geophys. Res.* 102 (1997) 2771–2787.
- [50] A.L. Thompson, Water in the Earth's upper mantle, *Nature* 358 (1992) 295–302.